a reprint from Applied Optics

Diffuse reflectance of oceanic waters: its dependence on Sun angle as influenced by the molecular scattering contribution

André Morel and Bernard Gentili

A spectral model of the inherent optical properties (absorption and scattering coefficients a and b, respectively) of oceanic case 1 waters with varying chlorophyll concentrations C is operated. It provides the initial conditions for Monte Carlo simulations aimed at examining the diffuse reflectance directly beneath the surface R and its variations with the solar zenith angle ζ. In most oceanic waters, molecular scattering is not negligible, and molecular backscattering may largely exceed backscattering. The variable contributions (depending on C and wavelength) of water molecules and particles in the scattering process result in considerable variations in the shape of the volume-scattering function. $R(\zeta)$ is sensitive to this shape. From the simulations, R (which increases as ζ increases) appears to be linearly related to $\cos \zeta$, with a slope that is strongly dependent on η_b, the ratio of molecular backscattering to particle backscattering. The value of the single-scattering albedo ($\varpi = b/a + b$) has a negligible influence on the $R(\zeta)$ function provided that $\varpi < 0.8$, a condition that is always fulfilled when dealing with oceanic case 1 waters. Practical formulas for $R(\zeta)$ are proposed. They include the influence of the diffuse sky radiation. The history of each photon and the number of collisions it experiences before exiting have been recorded. These histories and also a probabilistic approach allow the variations of R with $\cos \zeta$, η_b, and ϖ to be understood.

Introduction

The variabilities in the optical properties of oceanic case 1 waters have now been well analyzed, if not completely understood with respect to all possible causes of these variations. Following Smith and Baker,[1,2] bio-optical models have been developed, such as those recently published by Gordon et al.[3] and Morel[4]; they allow these properties, as well as the solar radiation propagation in the open ocean, to be predicted from knowledge of the phytoplanktonic pigment content. This content, generally expressed in terms of (chlorophyll a + pheophytin a) concentration, may vary in case 1 waters over a wide range, between, say, 0.01 and 10 mg m^{-3}, the low values (<1), however, being by far the most common. In such clear and rather oligotrophic waters, the bulk light-scattering process still remains, effected principally by the particulate material in suspension. These particles include various types of algal cells, all associated heterotrophic organisms feeding on them, and all debris created along the food chain or simply by natural death and decay. Scattering by water molecules, however, is definitely not negligible in these clear waters. In particular, molecular backscattering often exceeds the particle backscattering, as shown by Morel and Prieur,[5] and this fact is attested to by the blue color of many limpid oceanic waters. The enhanced influence of molecular scattering, when the backscattered flux is considered, obviously originates from the relative weakness of the backscattering efficiency of marine particulates compared with that of molecules.

The radiative regime within a water body, the decrease of solar radiant energy with increasing depth, the setting up of an upward flux, and globally the continuous rearrangement of the radiative field depend on the illumination conditions prevailing at the surface and on the three independent inherent optical properties of the medium (Preisendorfer[6]), namely, its absorption coefficient a, its (total) scattering coefficient b, and its volume scattering function $\beta(\theta)$, a function that expresses the angular distribution of the scattered flux as it results from a single-scattering process. (Symbols and definitions are those

The authors are with the Laboratoire de Physique et Chimie Marines, Université Pierre et Marie Curie, B.P. 08, F06230 Villefranche sur Mer, France.

Received 20 November 1990.
0003-6935/91/304427-12$05.00/0.

Table I. Significant Symbols, Definitions, and Units

Symbol	Definition	Unit
a	Total absorption coefficient	m^{-1}
a_w	Pure water absorption coefficient	m^{-1}
b	Total scattering coefficient	m^{-1}
b_b	Backscattering coefficient	m^{-1}
b_w	Pure water scattering coefficient	m^{-1}
b_p	Particle-scattering coefficient	m^{-1}
$\tilde{b}_b$	Backscattering probability (additional subscripts w and p for water and particle, respectively)	b_b/b
$\beta(\theta)$	VSF; no subscript = total, w and p subscripts for water and particles, respectively	$m^{-1}\,sr^{-1}$
$\tilde{\beta}(\theta)$	Phase function: $\beta(\theta)/b$ (subscripts w and p as above)	sr^{1}
c	Attenuation coefficient ($= a + b$)	m^{-1}
C	Pigment (Chl a + Pheo a) concentration	$mg\,m^{-3}$
$D(\theta)$	Scattering probability function	
E_d, E_u	Downwelling and upwelling irradiances on a horizontal surface	$W\,m^{-2}$
$\hat{E}_d$, $\hat{E}_u$	Downwelling and upwelling scalar irradiances	$W\,m^{-2}$
$\hat{E}$	(Total) scalar irradiance, $\hat{E} = \hat{E}_d + \hat{E}_u$	$W\,m^{-2}$
η	Ratio of molecular scattering to total scattering	b_w/b
η_b	Ratio of molecular backscattering to total backscattering	b_{bw}/b_b
L	Radiance; $L(\theta, \varphi)$ radiance distribution	$W\,m^{-2}\,sr^{-1}$
λ	Wavelength	nm
μ	Average cosine of the radiance distribution over all directions	$(E_d - E_u)/\hat{E}$
μ_d, μ_u	Average cosine for the downwelling or for the upwelling radiance distributions, respectively	$\mu_d = E_d/\hat{E}_d$ $\mu_u = E_u/\hat{E}_u$
$\tilde{\omega}$	Probability of photon survival (or single-scattering albedo)	b/c
p	Polarization factor for light scattered at a right angle (when incident light is unpolarized)	
p_1, p_2	Relative proportions of photons after 1, 2, . . . scattering events	
R	Reflectance (or irradiance ratio) = E_u/E_d	
ζ	Solar zenith angle (in air) and $\mu_0 = \cos\zeta$	
ζ'	Solar zenith angle in water, $\zeta' = \sin^{-1}(\sin\zeta/1.34)$, and $\mu_w = \cos\zeta'$	

of Morel and Smith[7]; they are summarized in Table I. The radiative field modification and its dependence on the inherent properties are rigorously expressed through the radiative transfer equation (RTE), which, in a differential form describes how the spatial distribution of radiances and their magnitude evolve along with depth. The shape of the volume-scattering function (VSF) is important in governing this evolution and, at each particular depth, in recasting the spatial structure of the radiative field.

At the particular depth zero, the upwelling flux, able to emerge from the ocean, is one particular aspect of the submarine radiative field that is also sensitive to the shape of the actual VSF. Gordon[8] recently has shown that the variation of the diffuse reflectance at null depth R with Sun angle is related to the VSF shape, a result that obviously could not have been obtained by Kirk,[9] who considered a unique VSF in his computations. Recall that R is defined as the ratio

$$R = E_u/E_d \tag{1}$$

of the upwelling to downwelling irradiances (and just beneath the surface in the present case).

Changes in shape of the VSF are to be expected in oceanic waters in relation to the relative importances of the molecular and particle scattering, which vary according to the particle concentration and thus the pigment concentration in case 1 waters. Throughout the spectrum, the relative importances of the molecular and the particle scattering also change since the λ dependence of water molecule scattering is much more pronounced than that due to particles. The impact of these VSF variations on R deserves a systematic study, the interest of which is obvious as remote sensing techniques rely on the behavior of the reflectance and on its interpretation. The RTE can be accurately solved through Monte Carlo simulations provided that sufficient computation time is available. A three-dimensional (3-D) code has been developed for several purposes. The present paper, based on the results of this simulation, is restricted to the examination of the problem as described above. First, the Monte Carlo computation is briefly presented, and then the model for the inherent optical properties of oceanic case 1 waters is provided before the presentation and discussion of the results.

Computational and Modeling Aspects

Monte Carlo Simulation

This method is similar to that used by Plass and Kattawar[10,11] and also by Gordon and Brown.[12] After a solar photon has been introduced just below the surface, its path is followed in the 3-D space throughout an ocean layer of a given thickness. Beyond the black bottom of this layer, photons are definitively lost. After each internal collision, each photon is assigned a weight that accounts for its partial absorption; i.e., its value is multiplied by $\tilde{\omega}$, which is the probability of photon survival. If it collides with the

air–sea interface, transmitted and reflected photons are weighted according to Fresnel law (including the possibility of total internal reflection). A photon history is terminated (and a new photon started) when its weight falls below a predetermined threshold (for example, 10^{-6}). For each collision in the medium, a random number (on 0–1) is generated and compared with the ratio $\eta = b_w/b$ to determine if the scattering event will be of a molecular type that due to a particle. The direction of the new trajectory with respect to the previous one is determined azimuthally by a random number (on 0–2π) and with a polar angle θ by another random number (on 0–1), which is compared to the cumulative scattering distribution or probability function $D(\theta)$.

In the case of molecular scattering by liquids, the phase function $\bar{\beta}_w(\theta)$ is expressed as (see, e.g., Kerker[13])

$$\bar{\beta}_w(\theta) = \frac{3}{4\pi(3+p)}(1 + p\cos^2\theta), \tag{2}$$

where θ is the scattering angle and p is the polarization factor, taken equal to 0.84 according to Morel.[14]

The cumulative scattering distribution $D(\theta)$ is defined (on 0–1) as being the progressive integral of the phase function

$$D(\theta) = 2\pi \int_0^\theta \bar{\beta}(\theta)\sin\theta d\theta,$$

so that by integrating Eq. (2), this distribution function for molecular scattering $D_w(\theta)$ turns out to be

$$D_w(\theta) = \frac{1}{2}\left[1 - \frac{\cos(\theta) + (p/3)\cos^3\theta}{1 + (p/3)}\right]. \tag{3}$$

The choice of the phase function for particulate scattering $\bar{\beta}_p(\theta)$ is discussed later when modeling the optical properties of oceanic waters [see Fig. 1(a) and curve p]. The related distribution function $D_p(\theta)$ is numerically computed from the discrete values $\bar{\beta}_p(\theta)$ and then fitted to a cubic spline function, shown in Fig. 1(b). With such continuous D_w and D_p distributions, all scattering angles are accessible, including those that are small. No angular averaging is done at this stage when computing the trajectories. Averaging occurs only at the detector level, when the photons are collected from various solid angles. There is no particular problem in multiplying the number of detectors for many depths and polar–azimuthal directions. There is only a practical limitation by the stochastic noise, if an insufficient number of photons are collected at the end of the simulation.

Statistical fluctuations are inevitable in any Monte Carlo computation. Their relative importance obviously diminishes for the increasing number of photons actually processed. The level of these fluctuations and consequently the significance (or the quality) of simulations carried out with diverse input parameters must be closely adjusted for further reliable comparisons.

In a strongly absorbing medium (with $\bar{\omega} = b/c$ very

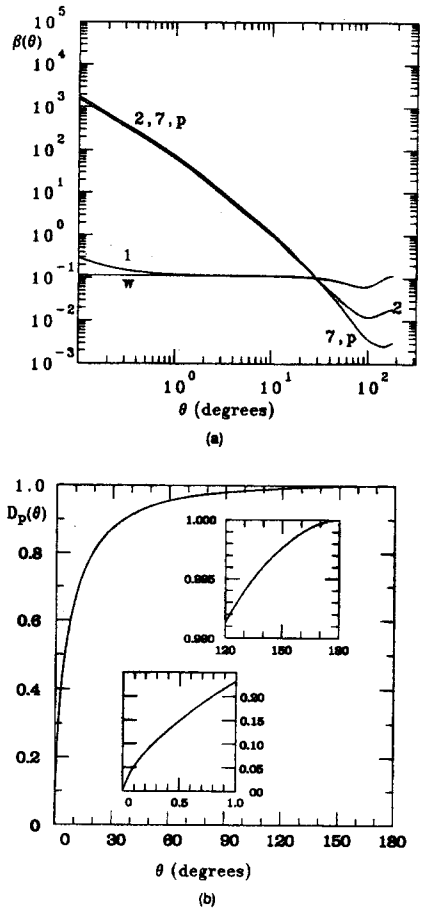

Fig. 1. (a) Phase functions for molecular scattering w [Eq. (2)] for particles p and for mixtures (1,2,7) with variable η values (see Table II). (b) Probability distribution function corresponding to the phase function adopted for particles; the insets show details of the small angle (0–1°) and large angle (120–180°) domains.

small), photons are quickly extinguished, the computation is fast, yet the radiant field is not properly created. Its creation is subordinated to the existence of a sufficient number of scattered photons still zigzagging within the medium. The converse proposition (long-living photons, a long computation, a well-constructed field) holds true for the opposite case of a quasi-conservative medium with $\bar{\omega}$ close to 1. To ensure the coherence within the results, the number of photons to be processed must therefore vary according to the $\bar{\omega}$ values. Within a layer of a given thickness and considering that enough photons must survive to build the light field, the product $N.n$, where N is the number of photons introduced and n is the average number of collisions they have experienced inside the layer, must be kept constant to create equally significant light fields. A photon finally disappears when its weight becomes less than t, the threshold value. This occurs after it has suffered n successive collisions so that

$$\bar{\omega}n \le t, \text{ then } n = \ln t/\ln(\bar{\omega}). \tag{4a}$$

If, for example, the euphotic layer is considered, the

downward flux that reaches its bottom is by definition 1% of that entering the surface. At this depth, the average weight of the remaining photons is also 1%. Therefore the mean number of scattering events they undergo before reaching this level is

$$\bar{n}_{euph} = \ln(10^{-2})/\ln(\bar{\omega}), \tag{4b}$$

even if for some photons the actual number of collisions can still be zero or much higher than $\bar{n}_{euph}$. At this level, and with the constraint of building an accurate radiative field within the layer considered, it is conceivable that photons having a weight below $t = 10^{-6}$ can safely be neglected. The resulting mean order of the scattering $\bar{n}$ value is

$$\bar{n} = -13.8/\ln(\bar{\omega}),$$

and the number N of photons to generate, inversely proportional to $\bar{n}$ for a predetermined quality in the results, is thus proportional to $-(\ln\bar{\omega})$. For the specific case of the euphotic layer (and also for the results presented here), the standard runs were carried out with a product of

$$N.n \sim 3.5 \times 10^8 \text{ (photons} \times \text{collisions)}.$$

For example, for $\bar{\omega} = 0.1$ and 0.9, the numbers of photons generated and then processed are 58 and 2.6×10^6, respectively. These high numbers are needed if azimuthal properties are also sought (not examined here). The proviso of equal quality entails approximately equal computation time, whatever the case and the $\bar{\omega}$ value envisaged.

The anticipated quality (in terms of stochastic noise) is also estimated from geometrical and physical viewpoints. This is easily done by determining whether the results satisfy rigorous relationships between the parameters of the radiative field. The exact and purely geometrical relationship,

$$R = (\mu_d - \mu)(\mu_u + \mu)^{-1}(\mu_u/\mu_d), \tag{5}$$

where μ_d and μ_u are the mean cosine for the downwelling and upwelling fluxes, respectively, and μ is the mean cosine for the entire field, tests the numerical consistency of the amount of photons counted in the collectors and of their cumulation (integrations over the radiance distribution to obtain various irradiances). The deviations from strict equality in this equation are less than 10^{-4} throughout the water column. The RTE itself (a physical relationship) can be verified under its integrated form (the divergence or Gershun equation):

$$a = \mathring{E}^{-1}d(E_d - E_u)/dz, \tag{6}$$

where $\mathring{E}$ is the scalar irradiance. The absorption coefficients, when recomputed from the three irradiances, do not differ from the initial values used as input by more than 0.5% and in general by 0.1% (except within the first upper and thin layer, or also when entering into the deepest layers remotely influenced by the artifactual presence of the black hole at the bottom, with $E_u \equiv 0$).

Modeling the Inherent Optical Properties of Oceanic Waters

The present model has been presented in detail in another paper[15]; it has much in common with that used by Gordon,[8,16] which essentially rests on the same source of data. The dependence of the (spectral) inherent properties on the chlorophyllous pigment concentration C is described by the following equations:

$$b(\lambda) = b_w(\lambda) + (550/\lambda)0.3(C)^{0.62}, \tag{7}$$

$$a(\lambda) = [a_w(\lambda) + 0.06A(\lambda)(C)^{0.65}][1 + 0.2Y(\lambda)], \tag{8}$$

with

$$Y(\lambda) = \exp - [0.014(\lambda - 440)], \tag{9}$$

$$c(\lambda) = a(\lambda) + b(\lambda). \tag{10}$$

The spectral values of the scattering and absorption coefficients for optically pure seawater, $b_w(\lambda)$ and $a_w(\lambda)$, are those of Morel[14] and Morel and Prieur,[5] respectively. The wavelength dependence of molecular scattering is conveniently expressed as a power law with an exponent of -4.32. Equation (7), already given by Gordon and Morel,[17] allows the scattering by particles to be inversely related to the wavelength and nonlinearly linked to the pigment content. Equation (8) and the $A(\lambda)$ values come from Prieur and Sathyendranath,[18] apart from a slight modification in the exponent value (0.65 instead of 0.602) for reasons explained by Morel.[15] The second set of brackets in this equation accounts for the covarying influence of locally formed yellow substances with a spectral absorption expressed [Eq.(9)] according to Bricaud *et al.*[19]

The inherent optical properties of oceanic case 1 waters are usefully summarized by Figs. 2 and 3, which show the loci corresponding to fixed values of the ratios $\bar{\omega}(\lambda)$ and of $\eta(\lambda) = b_w(\lambda)/b(\lambda)$ in the $(C) - (\lambda)$ plane. Both of these dimensionless quantities are essential in governing the radiative transfer. Also important in building up the in-water light field is the scattering phase function, which strictly results from an addition of the VSF for water molecules (subscript w) and the VSF for particles (subscript p), after due weighting by the appropriate ratio $\eta(=b_w/b)$; thus

$$\bar{\beta}(\theta) = \eta\bar{\beta}_w(\theta) + (1 - \eta)\bar{\beta}_p(\theta), \tag{11a}$$

where the λ dependency is omitted. In the Monte Carlo simulations, the actual VSF's for molecules and for particles are properly scaled by using their absolute values according to

$$\beta(\theta) = b\bar{\beta}(\theta) = b_w\bar{\beta}_w(\theta) + b_p\beta_p(\theta). \tag{11b}$$

The symmetrical phase function for pure water was

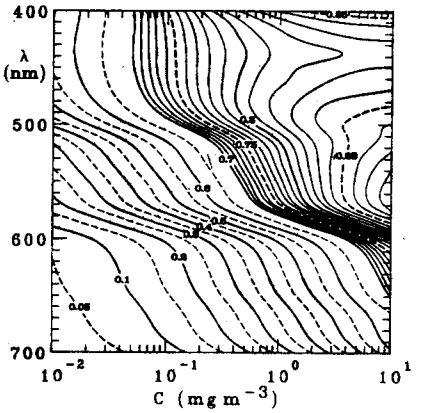

Fig. 2. Isopleths of $\bar{\omega}(= b/c)$ in the wavelength λ pigment concentration C plane, as computed through Eqs. (7)–(10).

given in Eq. (2). The forward peaked, strongly assymmetric phase function for particles was adopted from Petzold,[20] who determined this phase function in San Diego waters (station 2040) [see Fig. 1(a)]. Previous measurements reviewed by Morel[21] have demonstrated that, once the scattering by water is subtracted, the normalized particle-scattering function remains remarkably stable in shape, except perhaps in the backward directions, where measurements (never extended beyond 170°) are less reliable. The mean particle VSF for clear oceanic waters, as proposed by Morel,[21] was practically superimposable on those of Petzold for turbid waters. Besides this scientific argument, a practical advantage of this choice is the possibility of checking the present Monte Carlo simulation against others making use of the same VSF, namely, those of Kirk[9,22] and of Gordon *et al.*[8,12,23] (this VSF is labeled T).

The adoption of a single phase function for oceanic particulates undoubtedly, but inevitably, is a weakness. It contradicts other observations and subsequent modeling as that in Gordon and Morel,[17] which accounts for a variable backscattering efficiency by particles, in relation to the trophic state of the ocean water. When Petzold's VSF is adopted, the backscattering probability $\bar{b}_{bp}$ amounts to $\bar{b}_{bp} = b_{bp}/b_p = 0.0190$. This constant value is used to draw the isopleths of the ratio b_b/a in Fig. 4(a). More realistically, $\bar{b}_{bp}$ would be about 0.022 in clear, low-chlorophyll waters and would decrease regularly (logarithmically) with an increasing pigment concentration. An expression (compatible with the reflectance data) that was proposed by Morel[4] is used to construct Fig. 4(b). The isopleths exhibit palpable differences when compared with those in Fig. 4(a), particularly in the blue region and for high C. Such a change in $\bar{b}_{bp}$ necessarily implies a progressive modification of the particle phase function, which, however, is still largely unknown. That the nonalgal contribution decreases relative to the increasing pigment concentration and that the typical VSF of algal cells exhibits low $\bar{b}_b$ values[24,25] could be at the origin of this regular decrease of $\bar{b}_{bp}$. This explanation is still sufficient and comes up against another observation, which tends to demonstrate that algae are practically inoperative in the backscattering process (see the discussion by Morel and Ahn[26]). Therefore, with our present knowledge, the desirable adoption of two (or more) specific VSF's for different kinds of identified marine particle remains problematic, as acknowledged by Gordon.[8]

With a unique value for $\bar{b}_{bp}$ (=0.019) and by recalling that for molecular scattering $\bar{b}_{bw} = ½$, the relationships between η_b (=b_{bw}/b_b) and η (=b_w/b) are simply

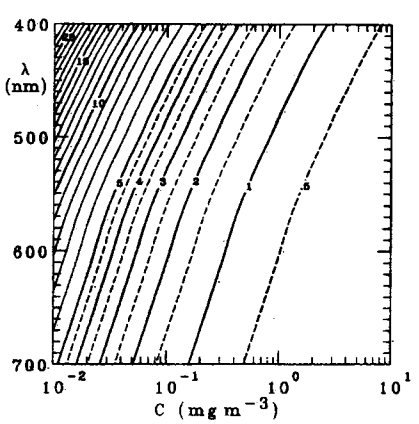

Fig. 3. As in Fig. 2 but for the isopleths of η (= b_b/b), expressed in percentages.

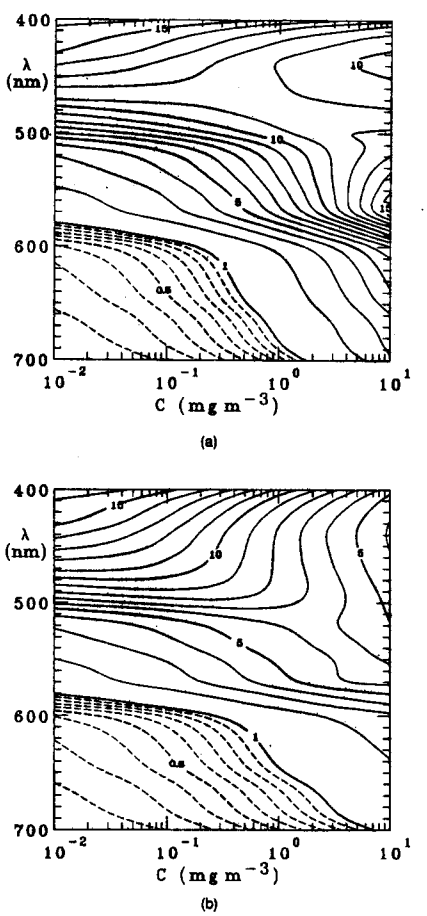

Fig. 4. (a) As in Fig. 2, but for the isopleths of b_b/a when the backscattering probability for particles $\bar{b}_{bp}$ is constant and equal to 1.90%. (b) As in (a) but $\bar{b}_{bp}$ varies with C according to the empirical equation given by Morel.[4]

expressed as

$$\eta_b = \eta[\eta + 0.038(1 - \eta)]^{-1} \quad (12)$$

and graphically presented in Fig. 5. For the η range that is typical of case 1 waters (Fig. 3), the corresponding η_b values are generally high, reaching about 80% for the clearest waters in the blue part of the spectrum. These values support the argument put forward in the Introduction where the importance (and even the predominance) of molecular backscattering in most oceanic situations was emphasized.

Selected Case Studies and Initial Conditions for the Simulations

Besides the initial conditions imposed at the ocean surface, the in-water radiative regime depends on the $\bar{\omega}$ ratio and on the phase function, itself ruled by the value of the η ratio. As an attempt to separate, if possible, the influences of these two parameters, two series of computations have been performed, the first by keeping $\bar{\omega}$ constant and changing η and the second by keeping η constant (a constant shape for the phase function), whereas $\bar{\omega}$ is variable. This choice is rendered easier owing to the approximate perpendicular disposition of the isopleths in Figs. 2 and 3, respectively. The selected cases in each series are situations in the real world, as shown in Fig. 6 (see the values in Table II). Some nonrealistic situations have been added for a full exploration and understanding of the problem; among these hypothetical situations, quasi-pure water, or suspended particles without water, obviously forms the limiting cases.

The initial lighting and sea-state conditions are as follows for systematic runs (other conditions have, with exception, been considered for sensitivity studies):

(1) The zenith–sun angle (ζ) varies between 0° and 80° (in air), and the photons, directly introduced beneath the surface, follow the corresponding refracted direction computed according to Snell's law

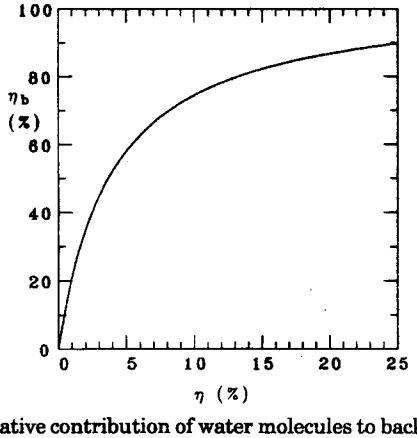

Fig. 5. Relative contribution of water molecules to backscattering η_b as a function of the relative contribution of water molecules to scattering η[Eq. (12)].

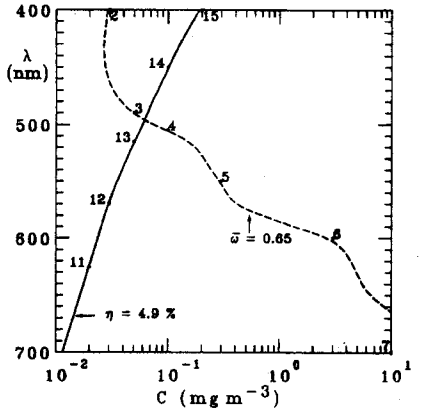

Fig. 6. As in Figs. 2 and 3 with the selected cases (numbered in reference to Table II) shown along with the closest isopleths for $\bar{\omega}(= 0.65)$ and $\eta(= 0.049)$.

(the refractive index of water is given a fixed value of 1.34).

(2) For systematic computations the Sun disk is given an angular diameter of 5° (instead of the actual value of 0°5 in air) to account approximately for the wavy interface of a calm sea with randomly oriented facets; more realistic air–sea interfaces have also been considered, and sensitivity tests have been effected by using an isotropic Gaussian distribution of sea surface slopes [Eqs. (1) and (2) in Cox and Munk[27]], which depends on the wind speed but omits the effect of wind directionality.

(3) The internal reflection coefficients at the water–air interface are interpolated between those tabulated by Austin[28] corresponding to a wind speed of 4 m s^{-1} or are computed from the Fresnel formula (for a flat or roughened ocean surface) with no significant differences ($< 0.1\%$) in the resulting reflectance values.

(4) An isotropic sky radiance distribution, with $L(\zeta)$ = constant, and a cardioidal distribution, with $L(\zeta) = L_o(1 + 2\cos\zeta)$, have also been systematically used for all cases considered.

Results

The ratio of the reflectances for various Sun–zenith angles ζ (in air) to the reflectance when $\zeta = 0$ is plotted as a function of $\cos\zeta$ in Fig. 7(a). The curves, from bottom to top (1–7), correspond to decreasing values of η; the lower curve is for pure water and the upper curve for almost pure particle scattering (η_b is still equal to 2%). The latter can be compared to, and actually agrees with, the results of Gordon[8] (with his phase function T, no molecular scattering, and $\bar{\omega} = 0.8$), which are replotted in Fig. 8(d). The straightforward conclusions are that the ζ dependence of R is highly variable in oceanic waters (the real cases 2–7 being only considered) and that these variations are regularly ordered according to the relative importance of the molecular scattering.

To first order, the magnitude of R, physically linked to the inherent properties, is ruled by the value of the ratio b_b/a [or of $b_b/(a + b_b)$], another ratio that comes

Table II. Selected Case Studies and Relevant Information

	λ (nm)	C (mg m^{-3})	b_w (m^{-1})	b_p (m^{-1})	a (m^{-1})	$\bar{\omega}$	η (%)	η_b (%)	$f_{diff,unif}$	$f_{diff,card}$
1	430	0	0.00550	1.E-7	0.01430	0.27778	99.99	100	0.312	0.309
2	400	0.03	0.00758	0.04691	0.02878	0.65438	13.91	81.0	0.336	0.329
3	490	0.05	0.00320	0.05256	0.02904	0.65755	5.74	61.6	0.367	0.358
4	505	0.1	0.00282	0.07838	0.04324	0.65252	3.47	48.6	0.382	0.372
5	550	0.3	0.00193	0.14221	0.07696	0.65192	1.34	26.3	0.401	0.389
6	600	3	0.00141	0.54344	0.28965	0.65291	0.26	6.40	0.418	0.402
7	700	10	0.00076	0.98262	0.71134	0.58026	0.077	1.99	0.410	0.394
11	625	0.02	0.00120	0.02335	0.32116	0.07101	4.888	57.49	0.371	0.364
12	570	0.03	0.00168	0.03292	0.07481	0.31624	4.855	57.32	0.372	0.365
13	515	0.05	0.00260	0.05001	0.05064	0.50954	4.942	57.77	0.373	0.365
14	450	0.1	0.00453	0.08796	0.03191	0.74349	4.898	57.54	0.369	0.358
15	400	0.2	0.00758	0.15208	0.04264	0.78928	4.748	56.74	0.363	0.359
16	400		0.00758	0.15208	0.0171	0.90326	4.748	56.74	0.330	0.325
17	400		0.01516	0.30416	0.0171	0.94917	4.748	56.74	0.278	0.276

from the quasi-single approximation, as developed by Gordon.[29] To put in evidence these relationships, the ratio of $R(\zeta)$ to either b_b/a [denoted f, Eq. (13)] or to $b_b/(a + b_b)$ [denoted f', Eq. (13′)] are shown in Figs. 7(b) and 7(c) and plotted as a function of μ_0 (=cos ζ).

The above curves [experiments 2–6 in Figs. 7(a)–7(c)] have all been obtained with a single value of $\bar{\omega}$ ($\simeq 0.65$, see Table II). At this stage it has not been proved that this parameter does not also play a role in the $R(\zeta)$ evolutions. Results obtained by Gordon[8] tend to demonstrate that $\bar{\omega}$ is also involved, since his two curves for pure particles [which are similar to the upper curve in Fig. 7(a)] and with almost the same phase function as used here differ when $\bar{\omega}$ increases from 0.8 to 0.9. The second set of simulations with η constant and $\bar{\omega}$ variable provides the possibility of answering this question. The results are shown [Figs. 8(a)–8(c)] in a way that is similar to that before. It can be observed that all curves for real situations [11–15 in Fig. 8(a)] almost coincide (within 2%). Interestingly, they all correspond to radiative regimes with $\bar{\omega}$ below 0.8 (from 0.07 up to 0.79). Only the curves for hypothetical cases, with $\bar{\omega} = 0.9$ or 0.95, increasingly depart from the quasi-common curve and in the same direction as in the numerical experiment of Gordon.[8] The $\bar{\omega}$ value of about 0.8 appears to be a kind of upper limit, beyond which the pattern of the $R - \zeta$ dependence abruptly changes. Another and more direct comparison with the results of Gordon has also been made by totally suppressing the molecular scattering and letting $\bar{\omega} = 0.9$. The agreement is satisfactory [curves 7′ and G.9 in Fig. 8(d)], when observing that the VSF in Gordon's and present simulations differ by some nuances.

From a practical viewpoint this result is important, as $\bar{\omega}$ in truly oceanic waters does not surpass this upper value (see Fig. 2); therefore the dependence of

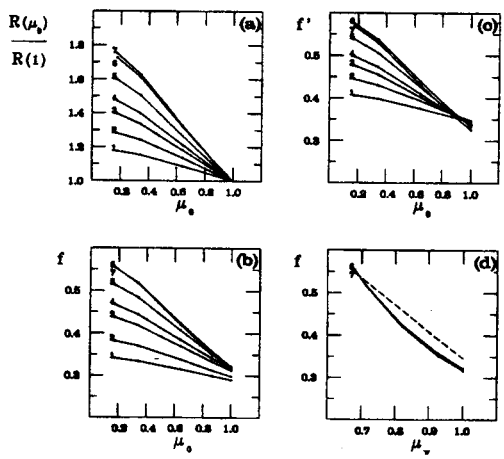

Fig. 7. (a) Ratio of the reflectances for various Sun–zenith angles (ζ) to the reflectance when $\zeta = 0$, plotted as a function of $\mu_0 = \cos \zeta$. The numbers in (a), (b), and (c) refer to those in Table II. (b) The f factor [Eq. (13)] as a function of μ_0. (c) The f' factor [Eq. (13′)] as a function of μ_0. (d) The f factor for cases 6 and 7 only as a function of $\mu_w = \cos \zeta'$ (in water) with $\zeta' = \sin^{-1}(\sin \zeta / 1.34)$; the dashed straight line was proposed by Kirk.[9]

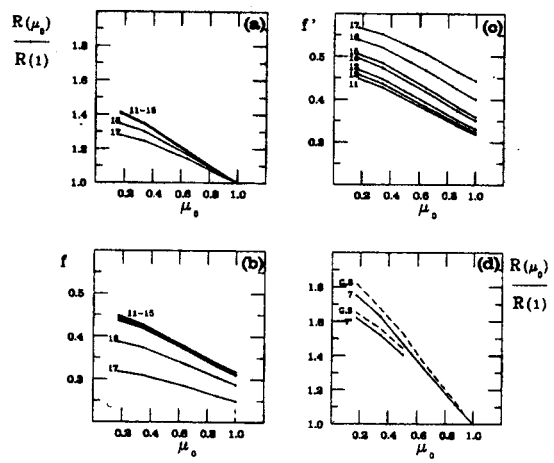

Fig. 8. (a)–(c) As in Figs. 7(a)–7(c) and for the other cases (11–17) are as in Table II. (d) As in (a) but for case 7 and a hypothetical case 7′ (not given in Table II) for which $\eta = 0$ and $\bar{\omega} = 0.9$. The dashed curves, G.8 and G.9, are redrawn from Fig. 2 of Ref. 8 for $\bar{\omega} = 0.8$ and 0.9, respectively.

$R(\zeta)$ on this parameter can be safely neglected (a conclusion no longer valid for coastal turbid waters). By writing the relationship between R and the ratio b_b/a as

$$R = f\frac{b_b}{a}, \tag{13}$$

its nonlinear character is accounted for by the possible variations in f as displayed in Figs. 7(b) and 8(b). This factor f is not dependent on $\bar{\omega}$, insofar as $\bar{\omega} < 0.8$, but depends only on ζ and η (or equivalently on μ_0 and η_b). An approximate formula, accurate within 1.5% if $\zeta < 70°$ (and 4% for $70° < \zeta < 80°$), can be used to account for these dependencies and is as follows:

$$f(\mu_0, \eta_b) = (0.6279 - 0.2227\eta_b - 0.0513\eta_b^2) + (-0.3119 + 0.2465\eta_b)\mu_0. \tag{14}$$

The possibility that R may also be expressed as a function of $b_b/(a + b_b)$ [Figs. 7(c) and 8(c)] does not imply a modification of the above empirical relationship. If R is now written as

$$R = f'\frac{b_b}{a + b_b}, \tag{13'}$$

there exists a straightforward relationship between f' and f:

$$f' = f\left(1 + \frac{b_b}{a}\right), \tag{14'}$$

which allows Eq. (14) to be used if f' and Eq. (13') are preferred.

Kirk[9] has computed $R(\zeta)$ for water where the VSF is constant and reduced to only the particle VSF. He then modeled the $R(\zeta)$ behavior as a function of μ_w, the cosine of the Sun–zenith angle inside water (refracted angle). This seems logical. However, R changes are presently found to be less linear when plotted versus μ_w than when plotted vs μ_0 [Fig. 7(d)]. Then μ_0 is adopted rather than μ_w in the above equation [Eq. (14)]. There are some discrepancies between Kirk's results and the present ones for water dominated by particles (case 7), in particular for high sun elevations. They could originate from the difference in the angular diameter of the sun (5° here, 0° in Ref. 9) or from the fact that, in Kirk's calculations, the internal Fresnel reflection is not accounted for (except if total). Sensitivity tests show that the present results are not substantially modified when using Kirk's hypotheses. The differences could also result from the cumulative distribution $[D_p(\theta)]$, which, however, is based on the same Petzold's VSF for particles but is used in the present simulation as a continuous function, whereas it is approximated by a step function (with 5° interval) in Kirk's simulation. Again tests for this effect do not show that R would be very sensitive to the way of modeling $D_p(\theta)$. Consequently, the origin of the (relatively small) differences between Kirk's results and our results remain unclear.

In a natural environment, the above variations of R with the solar elevation are smoothed by the effect of the diffuse sky radiation for which the corresponding reflectance is essentially constant. For cloudless skies, the diffuse radiations become in relative proportion more important when the Sun–zenith angle increases. Thus the enhanced R values, which occur at a low solar elevation, are actually reduced by the sky effect. The relative contributions of the Sun and sky in forming the total downwelling irradiance at the ocean surface E_{tot} depend on the wavelength and atmospheric conditions (namely, the aerosol content). These relative proportions can be expressed as

$$\alpha = E_{diff}/E_{tot}, \quad (1 - \alpha) = E_{dir}/E_{tot},$$

where E_{diff} is the diffuse irradiance originating from the sky dome and E_{dir} is the irradiance produced by direct Sun rays, with $E_{tot} = E_{diff} + E_{dir}$. It is easy to demonstrate that R, the reflectance for the total incoming radiation, is a linear combination of two reflectance values, R_{diff} and R_{dir}, pertinent to each kind of illumination, with the same coefficients as above, so that

$$R = \alpha R_{diff} + (1 - \alpha)R_{dir}. \tag{15}$$

For a given body of water, with a given value of b_b/a, the f factor in Eq. (13) can be written in the same way:

$$f = \alpha f_{diff} + (1 - \alpha) f_{dir}. \tag{15'}$$

Simulations performed with either a uniform or a cardioidal radiance distribution provide the f_{diff} values listed in Table II. The f values for any cloudless sky can be obtained by using successively Eq. (14) and then (15') as far as the relative proportions are known.

An even simpler method can be used. For each water body considered (for cases 2–7 and 11–15), the diffuse radiance distributions (uniform and cardioidal) lead to f_{diff} values numerically equal to f values, which would be observed for the sole Sun with certain angles in the air. These angles, ζ_{unif} and ζ_{card}, and their corresponding μ values, namely, $\mu_{unif} = 0.676$ and $\mu_{card} = 0.730$, are essentially stable whatever the water body considered. Then Eq. (14) can be used directly for the total (Sun + sky) radiation, provided that μ_0 is replaced by the following linear combination:

$$\mu_0 = \alpha\mu_{sky} + (1 - \alpha)\mu_{dir}, \tag{16}$$

where μ_{dir} is for the direct Sun as before, and μ_{sky} is one of the above μ_{unif} or μ_{card} values. Note that these average cosines differ from those directly derived from the sky radiance distributions in air (0.500 and 0.583, respectively) because of the angular compression caused by refraction.

Examples of real situations, combining Sun and

sky (assumed to be isotropic) according to their respective weight, are shown for wavelengths of 600 nm (case 6) and 400 nm (case 2) in Figs. 9 (a) and 9(b). The α values, which vary with the solar angle, have been computed by using the atmospheric model of Tanré *et al.*,[30] as operated by Morel,[15] with visibility values of 23 and 5 km. A duly weighted addition of the photons resulting from the Monte Carlo simulations, or the direct use of Eqs. (16) and then (14), give the same results (within 1%).

As expected, the enhanced f values occurring when ζ increases are smoothed by the increasing influence of the sky radiation at low Sun elevation. Conversely, the lower f values at high Sun elevations are raised by the inclusion of the diffuse component. This smoothing effect is (like α) spectrally variable and increases from the red to the blue part of the spectrum. It obviously is reinforced by increasing the atmospheric turbidity. The systematic examination of these intricate influences on f is beyond the scope of this paper.

The influence of the sea surface roughness, not yet examined, appears to be quite small as far as underwater reflectance is considered. According to Preisendorfer and Mobley[31] such an effect is expected to be maximal at low Sun altitudes and also if the optical properties of the water body already induce a notable dependence of R on changing ζ. This occurs when particle scattering dominates, as in cases 6 and 7 (Fig. 7 and Table II). In Figs. 9(c) and 9(d) are shown the results of a series of runs with an infinitely distant point light source combined with surface slope probabilities distributed according to an isotropic Gaussian function.[27] Compared to the previous standard computations, $R(\mu_0)$ or $f(\mu_0)$ is slightly increased; for case 7 and for $\zeta = 80°$ the maximal departures are +5 or +8% for wind speeds of 2.5 and 10 m s^{-1}, respectively. This rather weak effect obviously vanishes ($< 3.5\%$ at most) when the molecular scattering becomes preponderant as in case 2.

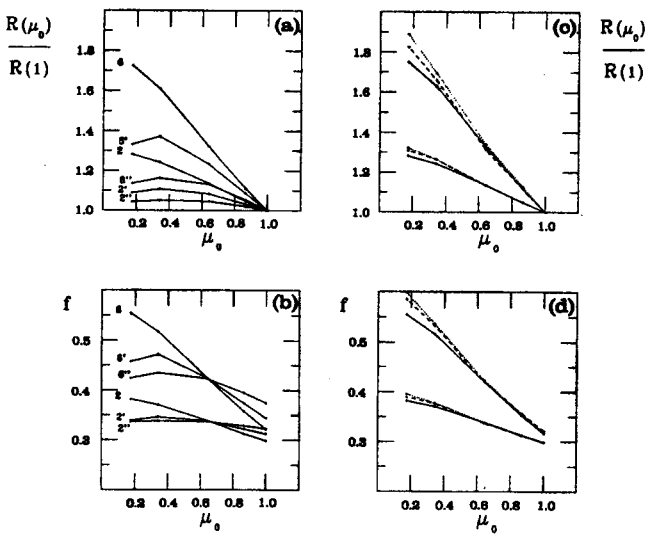

Fig. 9. (a) As in Fig. 7(a) except that only cases 2 and 6 are redrawn. In addition, the curves labeled 6′, 6″ and 2′, 2″ account for natural illumination conditions where sun and sky radiances are added according to their respective proportions (see text); 2′ and 6′ are for a visibility of 23 km, 2″ and 6″ for a visibility of 5 km. (b) As in Fig. 7(b); the curves are numbered as in (a). (c), (d) As in Figs. 7(a) and 7(b) but for cases 2 and 7 only and with varying wind speeds. The solid curves are redrawn from Figs. 7(a) and 7(b); the dashed and dotted curves are for 2.5 and 10 m s^{-1}, respectively, with corresponding wave slopes of $\pm 7°$ and $\pm 12.7°$ (at $\pm\sigma$).

Discussion

The dependence of the diffuse reflectance on the inherent optical properties of the medium is intuitively understood to result from the combination of two antagonistic processes. R is in some way proportional to the backscattering probability (b_b/c) and inversely proportional to the absorption probability (a/c); therefore it is proportional to b_b/a. Expressing the backscattering probability through the ratio b_b/c, however, is an oversimplification, at least for two reasons. Even in the case of single scattering (a situation approached when $\tilde{\omega}$ is small), the forward-scattering lobe is also, at least partly, involved as soon as the entering photons are not all traveling along the vertical direction (see, e.g., Stavn and Weidemann[32]). When multiple scattering occurs, backscattered and also forward-scattered photons are involved in forming the upward stream. In the classical Eq. (13), b_b is by approximation used to replace a variable and unknown portion of the VSF where the backward lobe, after various convolutions, often has a major, albeit not exclusive, role. This approximation results in a nonconstant f factor in this equation. For example, in Morel and Prieur[5] this equation was initially written

$$R = 0.33(1 + \Delta)(b_b/a)$$

with a corrective term $\Delta(= \pm 5\%)$ accounting for various incident radiance distributions, radiative regimes, and also VSF's (Prieur[33]). Recent work,[8,9] including the present one, tends to show that the possible variations of the above coefficient are wider (between 0.25 and 0.55), at least if hypothetical situations (a sun in a black sky) are considered. The direction and magnitude of these variations deserve examination.

The first question, raised by Fig. 7(b), concerns the sensitivity of the $f(\mu_0)$ function to the molecular contribution depicted by the ratio η_b; it can be answered at least empirically. The molecules intervene with a symmetrical, almost isotropic, scattering function. The orientation of the Sun rays is less important with a round-shaped VSF than it can be with a strongly asymmetrical function, e.g., that typical of particles. When particle scattering is predominant, the lateral portion of the VSF becomes increasingly involved when ζ increases. Consequently, an enhancement of the upward flux is clearly put in evidence by the present simulations. This explanation, however, supposes that single scattering (or scatterings of the first orders) dominates in the ascending flux, which in turn supposes that $\tilde{\omega}$ is not too high.

The probability of scattering events of the nth order is as $\bar{\omega}^n$ and thus can remain high for high orders, only if $\bar{\omega}$ is near 1. In such a case a multiple-scattering regime prevails even in the upper layers, which results in many convolutions of the VSF with itself and finally in a scattered light field tending to be isotropic. Therefore such a highly diffuse field becomes less dependent on the solar elevation. This evolution is put in evidence by Fig. 8(b), where the VSF (or η_b) is kept unchanged, whereas $\bar{\omega}$ is given increasing values. The f curves, practically superimposable as long as $\bar{\omega}$ goes from 0.07 to 0.79 (curves 11–15), suddenly start to deviate when $\bar{\omega}$ exceeds 0.8 (curves 16 and 17), and the f factor tends to be lower, i.e., less influenced by the Sun elevation.

More insight can be gained in studying the histories of the emerging photons. The depths they have reached and, more interesting for the present purpose, the number n of collisions each of them has undergone before exiting have been recorded. Within the whole population of exiting photons, the relative proportions, $p_1, p_2, \ldots, p_n$, of those having experienced 1, 2, . . . , n scattering events can be identified and displayed (see Fig. 10). Also an average number of collisions, typical of this population, can be computed as being the following weighted sum:

$$\bar{n} = p_1 + 2p_2 + \ldots + np_n . \tag{17}$$

Actually the series of p_n numbers (with $\Sigma p_n = 1$), as well as the average number $\bar{n}$, can be predicted in a simple, albeit not rigorous, way. (The approximation consists of assuming that the probability distributions for various orders of scattering within the emerging photon population is identical to that inside the medium.) In the scattered light field established in the upper layer and with the successive scattering probabilities varying as $\bar{\omega}^n$, the relative proportions of photons having experienced 1, 2, . . . , n scatterings, $p_1, p_2, \ldots, p_n$, are expressed as

$$p_n = \bar{\omega}^n \Big/ \sum_1^\infty \bar{\omega}^n ,$$

where $\Sigma_1^\infty \bar{\omega}^n$ is the sum of all probabilities; i.e., it represents the entire population of photons, no matter how many times they have interacted. This sum being equal to $\bar{\omega}/(1 - \bar{\omega})$ the relative proportions p_n are therefore

$$p_n = \bar{\omega}^{n-1}(1 - \bar{\omega}) . \tag{18}$$

The Monte Carlo simulations show (Fig. 10) that these relative numbers p_n of exiting photons having undergone 1, 2, . . . , n scattering events follow closely the above geometric progression [Eq. (18)]. The agreement slightly degrades for those photons returning from deeper layers after many interactions (more than 20, see cases 16 and 17 in Fig. 10).

The average number of collisions $\bar{n}$, which characterizes the upward photon flux, obtained by combining Eqs. (17) and (18), turns out to be

$$\bar{n} = 1/(1 - \bar{\omega}) . \tag{19}$$

This hyperbolic expression with respect to $\bar{\omega}$ is also well verified through the simulations (Fig. 11). The asymptotic behavior of $\bar{n}$ when $\bar{\omega}$ approaches 1 explains the rapid change of the $f(\mu_0)$in such highly diffusing media. Note that $\bar{n}$ in Eq. (19) can also be written $\bar{n} = (a/c)^{-1}$ and thus is the reciprocal of the probability of photon absorption. We have not been

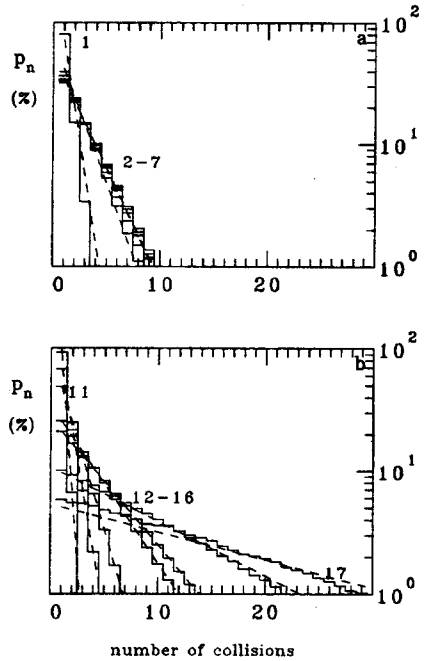

Fig. 10. Relative proportions p_n (in percentages and with a log scale) of exiting photons having experienced a given number of collisions (n, from 1 to 30). The solid stepped curves are for the results of Monte Carlo computations; the dashed continuous curves are for predictions from Eq. (18). (a), (b) The two sets of computations are numbered as in Table II.

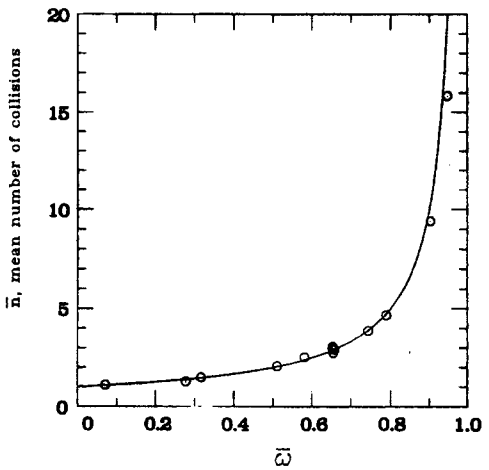

Fig. 11. Average number $\bar{n}$ of collisions [computed according to Eq. (17)] experienced by the entire population of emerging photons as a function of the ratio $\bar{\omega}$. The hyperbola corresponds to the predictions of Eq. (19), and the circles are the results of Monte Carlo experiments.

able to find a reference to such a simple result in the literature, although it is likely that it has been obtained in the past.

Summary and Conclusions

A spectral model of the inherent optical properties of oceanic case 1 waters, accounting for their dependence on the phytoplanktonic pigment content C, is used in conjunction with a Monte Carlo simulation to derive the variations of the diffuse reflectance R with the Sun–zenith angle ζ (in air) or its cosine μ_0. In certain conditions ($\zeta < 70°$), these variations are linearly related to μ_0, with a slope that depends on the shape of the phase function. This shape is strongly influenced by molecular scattering, which plays an important role in most oceanic waters and even a dominant role when the backward directions are considered. Therefore the slope changes to be expected are in no way negligible from one water body to another. They also may occur for a given water body when the wavelength changes, since such a change modifies the respective contributions of particles and molecules in the global-scattering process

In reflectance models these variations with respect to both μ_0 and η_b have been ignored as well as in the interpretation of field measurements of R. Part of the variability as observed in the R–C relationship could originate from this effect, while until now it has been entirely attributed to the variable nature of the absorption and scattering capabilities of algae (and of their debris or other associated particles). These field data and the subsequent models are the basis on which rest the techniques and algorithms developed for the interpretation of the ocean color as remotely detectable. The varying f factor (through which R and b_b/a are related) actually does not explicitly appear in any algorithm in use for remote sensing data. It is, however, implicitly involved when discriminating between case 1 waters and turbid case 2 waters (Bricaud and Morel[34]) and, more generally, when forming the ratio of two marine signals received at two wavelengths (which implies an f factor that is insensitive to λ).

In spite of the ignorance about this f effect, the reason the remotely sensed ocean color has nevertheless been successfully processed and interpreted lies in a favorable conjunction of approximately parallel evolutions of two geometrical quantities, namely, the f factor and the Q factor. This second factor relates the upwelling radiance L_u to the upwelling irradiance E_u, according to $L_u = E_u/Q$, where Q ($= \pi$ for a Lambertian reflector) is above π for oceanic water and may vary. It intervenes because a remote sensor detects radiance and not irradiance (or reflectance). Therefore the water-leaving radiance, in its normalized form (Gordon and Clark[35]), for example, is expressed through an equation that explicitly contains the ratio R/Q or, for a given water and given b_b/a value, contains the ratio f/Q. As was pointed out by Gordon,[8] the similar trends of f and Q with solar elevation result in an approximate stability in their ratio. This question, however, is more complex, especially because the Q factor cannot be straightforwardly averaged and its zonal and azimuthal dependencies cannot be disregarded. In the perspective of multiangle imaging sensors, the bidirectional aspect of the ocean reflectance still deserves further research.

This work was jointly supported by the Centre National de la Recherche Scientifique (UA 353) and by the Agence Spatiale Européenne (contract ESTEC 9111/90/NL-PR).

References

1. R. C. Smith and K. S. Baker, "The bio-optical state of ocean waters and remote sensing" Limnol. Oceanogr. **23,** 247–259 (1978).
2. R. C. Smith and K. S. Baker, "Optical classification of natural waters and remote sensing," Limnol. Oceanogr. **23,** 260–267 (1978).
3. H. R. Gordon *et al.*, "A semianalytic radiance model of ocean color," J. Geophys. Res. **93,** 10909–10924 (1988).
4. A. Morel, "Optical modelling of upper ocean in relation to its biogenous matter content (Case 1 waters)," J. Geophys. Res. **93,** 10,749–10,768 (1988).
5. A. Morel and L. Prieur, "Analysis of variations in ocean color," Limnol. Oceanogr. **22,** 709–722 (1977).
6. R. W. Preisendorfer, "Application of radiative transfer theory to light measurements in the sea," Monogr. Int. Union Geod. Geophys. Paris, **10,** 11–30 (1961).
7. A. Morel and R. C. Smith, "Terminology and units in optical oceanography," Mar. Geod. **5,** 335–349 (1982).
8. H. R. Gordon, "Dependence of the diffuse reflectance of natural waters on the sun angle," Limnol. Oceanogr. **34,** 1484–1489 (1989).
9. J. T. O. Kirk, "Dependence of relationship between inherent and apparent optical properties of water on solar altitude," Limnol. Oceanogr. **29,** 350–356 (1984).
10. G. N. Plass and G. W. Kattawar, "Radiative transfer in an atmosphere–ocean system," Appl. Opt. **8,** 455–466 (1969).
11. G. N. Plass and G. W. Kattawar, "Monte-Carlo calculations of radiative transfer in the earth's atmosphere ocean system: I, Flux in the atmosphere and ocean," J. Phys. Oceanogr. **2,** 139–145 (1972).
12. H. R. Gordon and O. B. Brown, "Irradiance reflectivity of a flat ocean as a function of its optical properties," Appl. Opt. **12,** 1549–1551 (1973).
13. M. Kerker, *The Scattering of Light and Other Electromagnetic Radiation* (Academic, New York, 1969), p. 666.
14. A. Morel, "Optical properties of pure water and pure seawater," N. G. Jerlov and E. Steemann Nielsen, Eds. in *Optical Aspects of Oceanography* (Academic, New York, 1974), pp. 1–24.
15. A. Morel, "Light and marine photosynthesis: a model with geochemical and climatological implications," Prog. Oceanogr. **26,** 263–306 (1991).
16. H. R. Gordon, "Bio-optical model describing the distribution of irradiance at the surface resulting from a point source embedded in the ocean," Appl. Opt. **26,** 4133–4148 (1987).
17. H. R. Gordon and A. Morel, *Remote Assessment of Ocean Color for Interpretation of Satellite Visible Imagery; a Review,* (Springer-Verlag, New York, 1983).
18. L. Prieur and S. Sathyendranath, "An optical classification of coastal and oceanic waters based on the specific absorption of phytoplankton pigments, dissolved organic matter, and other particulate materials," Limnol. Oceanogr. **26,** 671–689 (1981).

19. A. Bricaud, A. Morel, and L. Prieur, "Absorption by dissolved organic matter of the sea (yellow substance) in the UV and visible domains," Limnol. Oceanogr. **26,** 43–53 (1981).
20. T. J. Petzold, "Volume scattering functions for selected natural waters," SIO Ref. 72–78 (Scripps Institution of Oceanography, San Diego, Calif., 1972).
21. A. Morel, "Diffusion de la lumière par les eaux de mer; résultats théorique et approche théorique," in *Optics of the Sea,* AGARD Lect. Ser. Sec. 3 **63,** 1–76 (1973).
22. J. T. O. Kirk, "Monte Carlo study of the nature of the underwater light field in, and the relationships between optical properties of, turbid yellow waters," Aust. J. Mar. Freshwater Res. **32,** 517–532 (1981).
23. H. R. Gordon, O. B. Brown, and M. M. Jacobs, "Computed relationships between the inherent and apparent optical properties of a flat homogeneous ocean," Appl. Opt. **14,** 417–427 (1975).
24. A. Morel and A. Bricaud, "Theoretical results concerning the optics of phytoplankton, with special reference to remote sensing application," in *Oceanography from Space* (Plenum, New York, 1981), pp. 313–327.
25. A. Bricaud, A. Morel, and L. Prieur, "Optical efficiency factors of some phytoplanktons," Limnol. Oceanogr. **28,** 816–832 (1983).
26. A. Morel and A. Y. Ahn, "Optics of heterotrophic nanoflagellates and ciliates: a tentative assessment of their scattering role in oceanic waters compared to those of bacterial and algal cells," J. Mar. Res. **49,** 177–202 (1991).
27. C. Cox and W. Munk, "Some problems in optical oceanography," J. Mar. Res. **14,** 63–78 (1955).
28. R. W. Austin, "The remote sensing of spectral radiance from below the ocean surface," in *Optical Aspects of Oceanography,* N. G. Jerlov and E. Steemann Nielsen, eds. (Academic, New York, 1976), pp. 317–344.
29. H. R. Gordon, "Simple calculation of the diffuse reflectance of the ocean," Appl. Opt. **12,** 2803–2804 (1973).
30. D. Tanré, M. Herman, P. Y. Deschamps, and A. de Leffe, "Atmospheric modeling for space measurements of ground reflectances including bidirectional properties," Appl. Opt. **18,** 3587–3594 (1979).
31. R. W. Preisendorfer and C. D. Mobley, "Albedos and glitter patterns of a wind-roughened sea surface," J. Phys. Oceanogr. **16,** 1293–1316 (1986).
32. R. H. Stavn and A. D. Weidemann, "Shape factors, two-flow models and the problem of irradiance inversion in estimating optical parameters," Limnol. Oceanogr. **34,** 1426–1441 (1989).
33. L. Prieur, "Transfert radiatif dans les eaux de mer: application à la détermination des paramètres optiques caractérisant leur teneur en substances dissoutes et particulaires," *Thèse d'Etat* (Université Pierre et Marie Curie, Villefranche sur Mer, France, 1976).
34. A. Bricaud and A. Morel, "Atmospheric corrections and interpretation of marine radiances in CZCS imagery; use of a reflectance model," Oceanol. Acta **7,** 33–50 (1987).
35. H. R. Gordon and D. K. Clark, "Clear water radiances for atmospheric correction of coastal zone color scanner imagery," Appl. Opt. **20,** 4175–4180 (1981).